Arch. Metall. Mater. **67** (2022), 4, 1481-1486

DOI: https://doi.org/10.24425/amm.2022.141078

MYEONGJUN JI[1], EUNG RYONG KIM[1], MI-JEONG PARK[1], HEE YEON JEON[1], JAEYUN MOON[2], JONGMIN BYUN[1], YOUNG-IN LEE[1*]

SIMPLE SYNTHESIS OF BLACK TiO_2 NANOFIBERS VIA CALCINATION IN INERT ATMOSPHERE

Black TiO_2 nanofibers have recently emerged as a promising material that has both advantages of black metal oxide and one-dimensional nanostructure. However, current reduction-based synthesis approaches are not compatible with practical applications because these processes require high process costs, complicated processes, and sophisticated control. Therefore, it is still necessary to develop a simple and facile method that can easily introduce atomic defects during the synthesis process. This work suggests an electrospinning process with an antioxidant and subsequent calcination process for the facile synthesis of black TiO_2 nanofibers. The synthesized black TiO_2 nanofiber has an average diameter of 50.3 nm and a rutile structure. Moreover, this nanofiber represented a noticeable black color and a bandgap of 2.67 eV, clearly demonstrating the bandgap narrowing by the introduced atomic defects.

Keywords: Black TiO_2, Nanofibers, Electrospinning, Calcination, Atmosphere

1. Introduction

One-dimensional (1D) oxide nanofiber that has a high aspect ratio and specific surface area has attracted enormous attention in various photoelectrochemical applications due to dimensionality for easily separating electron-hole pairs and large active sites [1,2]. Among the various oxide materials, the black TiO_2 that contains a surface disordering region and a crystalline core has been regarded as one of the most promising materials in various applications such as visible-light-driven environmental remediation, water splitting, energy storage, and photothermal conversion due to its superior properties induced by atomic defects in a disordering region [3-6].

Since the pioneering report of Chen and Mao on the subsequent hydrogenation methods for black TiO_2 nanoparticles received much attention [4], there have been many efforts to develop a facile synthesis strategy for black TiO_2 nanoparticles. The partial reduction method of pre-synthesized white TiO_2 nanofibers using hydrogenation and high energy processes is a general method for the synthesis of black TiO_2 nanoparticles. However, these methods have some drawbacks such as high process cost, a prolonged reaction time, and sophisticated and harsh experimental conditions to introduce atomic defects [7-11]. Recently, in order to overcome the drawbacks of the partial reduction process, the controlled oxidation process has been reported, which induces the defects without an additional reduction process during nucleation and growth steps of species by blocking oxygen atoms or using chemical antioxidants [12-16]. However, almost all solution-based processes have limitations in controlling the chemical bonding with oxygen during the growth process into fibrous form, so there is no report on the facile synthesis method for black TiO_2 nanofibers using this concept without post-treatment. Therefore, there are still remaining challenges in the development of a simple synthesis method for black TiO_2 nanofibers.

In the present work, we suggest a simple and facile synthesis of black TiO_2 nanofibers induced oxygen vacancies and Ti^{3+} defects. The central concept is that atomic defects occur in polymeric nanofibers with antioxidants during nucleation and growth steps of TiO_2 and further oxidation is inhibited utilizing an oxygen-deficient atmosphere. For this purpose, the electrospun nanofibers containing precursors were calcined in the Ar atmosphere. To the best of our knowledge, this is the first report that uses electrospinning process for the synthesis of black TiO_2 nanofibers without a reduction process.

[1] SEOUL NATIONAL UNIVERSITY OF SCIENCE AND TECHNOLOGY, DEPARTMENT OF MATERIALS SCIENCE AND ENGINEERING, SEOUL, 01811, REPUBLIC OF KOREA
[2] UNIVERSITY OF NEVADA, DEPARTMENT OF MECHANICAL ENGINEERING, LAS VEGAS, 4505 S. MARYLAND PKWY LAS VEGAS, NV 89154, UNITED STATES

* Corresponding author: youngin@seoultech.ac.kr

2. Experimental

Titanium tetraisopropoxide [TTIP, $Ti[OCH(CH_3)_2]_4$, 99.99%], polyvinyl pyrrolidone (PVP, M_w = 1 300 000, 99.9%), acetic acid, citric acid, and anhydrous ethyl alcohol were purchased from Sigma-Aldrich (St. Louis, MO, USA) and were directly used as they were received without any further purification. The viscous electrospinning solutions were prepared by dissolving 0.45 g of polyvinylpyrrolidone (PVP, Mw: 1,300,000) and 1.5 g of titanium tetraisopropoxide in 12 ml of ethanol under vigorous stirring at a rate of 200 rpm for 1 h, ensuring that all chemicals have dissolved. Then, 3 ml of acetic acid was added to alleviate the hydrolysis reaction of the titanium precursor and 1.5 g of citric acid was further added as an antioxidant and totally dissolved.

The solution was transferred into syringes attached needle adaptor with a 0.25 mm inner diameter needle. A rotating metal collector covered by an aluminum foil was used as the cathode collector and the distance between the nozzle tip and collector was fixed at 12 cm. The precursor solution was injected through a syringe pump (KDS200, KD Scientific Inc., Holliston, MA, USA) controlled at a rate of 0.3 $ml \cdot h^{-1}$ and the solution was negatively electrified at 20 kV by a power supply (HV60, NanoNC Co., Ltd, Seoul, Korea). The as-spun nanofibers were calcined at 700°C for 6 h with a heating rate of 5°C/min in air and Ar atmosphere to remove PVP and crystallize into TiO_2.

The crystal structure of the obtained nanofibers was characterized by X-ray diffraction (XRD, X'Pert Powder, Malvern Panalytical, Almelo, Netherlands). The crystallite size was calculated by Scherrer's equation from XRD patterns. Raman spectra were obtained by a LabRAM HR spectrometer (HORIBA Jobin Yvon, France) with an excitation wavelength of 514 nm to investigate the structural variation. The morphology and microstructure of the nanofibers were analyzed by field-emission scanning electron microscopy (FE-SEM, S-4800, Hitachi, Ibaraki, Japan) and transmission electron microscope (TEM, JEM-2100F, JEOL, Tokyo, Japan). The average diameters and size distribution were determined by manually selecting and measuring around 200 nanofibers from obtained micrographs using software ImageJ. The variation of chemical bonding was analyzed using X-ray photoelectron spectroscopy (XPS, K-Alpha+, Thermo Fisher Scientific, United States). The optical absorbance and diffuse reflectance spectra were recorded on a UV-vis spectrophotometer (SHIMADZU UV-2600, SHIMADZU Japan) equipped with an integrated sphere, using $BaSO_4$ as a reference. The bandgap energy of the synthesized nanofibers was calculated by the Kubelka-Munk function from the diffuse reflectance spectra.

3. Results and discussion

The morphology of as-spun nanofibers with or without citric acid, represented in Fig. 1(a,d), are piled up randomly oriented in nonwoven form and show a well-defined fibrous structure with a smooth surface with an aspect ratio of over several thousand. After the calcination process in Air (Fig. 1(b,e)) or Ar (Fig. 1(c,f)) atmosphere, all nanofibers maintain the initial fibrous structure with a high aspect ratio. However, a rougher surface and smaller average diameter than as-spun nanofibers are observed (Fig. 2). It is attributed to the removal of polymer matters and the crystallization into TiO_2 during the calcination process, resulting in the shrinkage of total volume with the formation of primary particles [17]. The digital photographs (inset of Fig. 2) clearly present the effect of the atmosphere during the calcination. The colors of both nanofibers calcined in the air atmosphere are white regardless of the addition of citric acid. On the other hand, the nanofibers calcined in the Ar atmosphere respectively have gray and black colors. The change of color suggests the introduc-

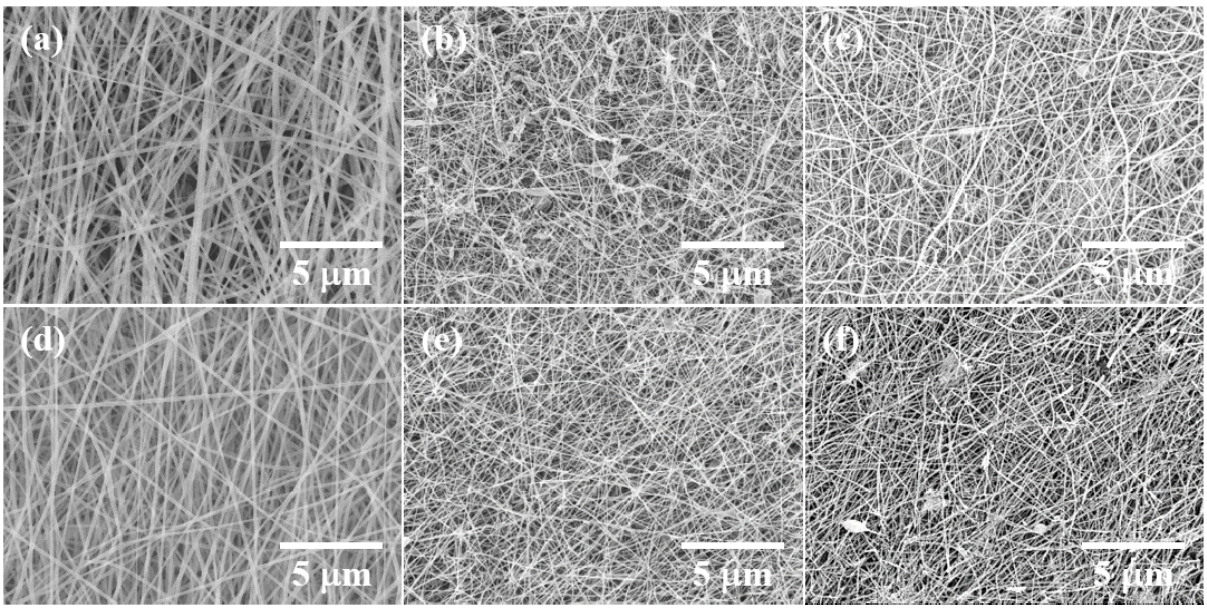

Fig. 1. Low magnification FE-SEM images of (a,b,c) nanofibers non-containing citric acid and (d,e,f) nanofibers containing citric acid: (a,d) as-spun nanofibers, (e,f) calcined nanofibers in air atmosphere, (c,f) nanofibers in Ar atmosphere

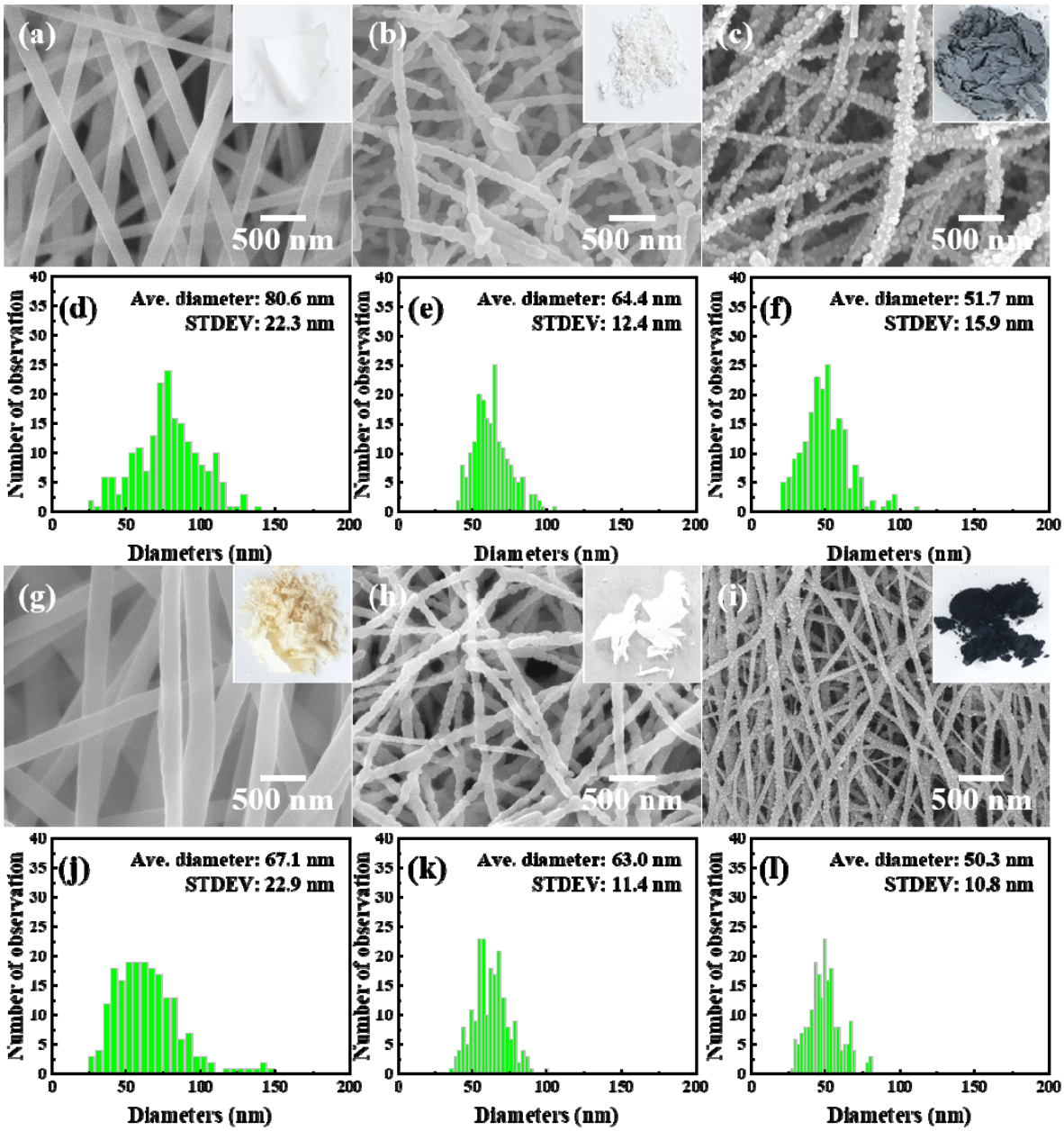

Fig. 2. High magnification FE-SEM images of (a,b,c) nanofibers non-containing citric acid and (g,h,i) nanofibers containing citric acid, and digital images of the corresponding samples (inset of FE-SEM image). The graphs showing the size distribution of (d,e,f) nanofibers non-containing citric acid and (i,k,l) nanofibers containing citric acid: (a,d,g,j) as-spun nanofibers, (b,e,h,k) calcined nanofibers in air atmosphere, (c,f,i,l) nanofibers in Ar atmosphere

tion of oxygen vacancies by the incomplete oxidation of TiO_2 nanofibers, because oxygen vacancies form the intermediate state in the energy forbidden region and extend the absorption spectrum [1,2,11]. Furthermore, the darker color of nanofibers containing citric acid indicates that citric acid actively inhibits the oxidation process of nanofibers (Fig. 2(i)).

The crystal structure of the obtained white, gray, and black nanofibers was investigated by X-ray diffraction patterns and the results are exhibited in Fig. 3(a). All nanofibers have only the TiO_2 crystal structures without the impurity phases. The white-colored nanofiber has a composite structure that is consisted of anatase (JCPDS No. 21-1275) and rutile (JCPDS No. 21-1276) phases but, the gray and black nanofibers only have the rutile phases of TiO_2. The difference in the crystal structure of nanofibers calcined in air and the Ar atmosphere is ascribed that oxygen vacancies are formed during the initial crystallization in the Ar atmosphere, which can lead to accelerated phase transformation from anatase into the rutile phase by the decrease of activation energy [18-20]. Furthermore, the diffraction patterns of black TiO_2 nanofibers exhibit lower diffraction intensity than that of gray nanofibers in spite of the similar average diameter (Fig. 2(f,l)) and crystallite size (TABLE 1) of both samples. Alleviation of intensity indicates the high concentration of oxygen vacancies in black TiO_2 nanofibers because oxygen vacancies are crystallographic defects that disrupt the periodic arrangement of crystals [9,11].

TABLE 1

Crystallites sizes of calcined TiO_2 nanofibers calculated by Scherrer's equation

Nanofibers	hkl	2Θ (degree)	FWHM (rad)	Crystallite size (nm)
Gray TiO_2 NFs	110	27.481	0.00724	19.71
	101	36.120	0.00761	19.17
	111	41.358	0.00880	16.85
	211	54.360	0.00848	18.38
Black TiO_2 NFs	110	27.417	0.00962	14.84
	101	35.998	0.00946	15.41
	111	41.241	0.00813	18.21
	211	54.357	0.00942	16.54

Raman spectroscopy was conducted to examine in detail the structural variation of calcined nanofibers according to the atmosphere and chemical agent. As shown in Fig. 3(b), the four characteristic peaks of rutile phase, which are located at 142, 239 446, and 610 cm^{-1}, are clearly observed in all nanofibers [21]. However, it is widened and weakened most peaks of gray and black nanofibers than a white nanofiber. As previously reported, this change is associated with the breaking down of the symmetry of the TiO_2 crystal and the local disordering that originated from the oxygen vacancies [8,22,23]. The detailed investigation of the microstructure of gray and black TiO_2 nanofibers was conducted through TEM analysis, shown in Fig. 3(c-h), in which is clearly observed the individual fibrous form constructed by nanoscale crystallites fully bonded with neighboring crystallites. The lattice fringe with the interplanar spacing of 0.324 nm corresponding to (110) plane of rutile TiO_2 is distinctly observed in HR-TEM images of both TiO_2 nanofibers (Fig. 3(d,g)). However, the disordered region, which is the typical structural feature of black TiO_2, on the surface is only observed in HR-TEM images of black TiO_2 nanofibers [4,22].

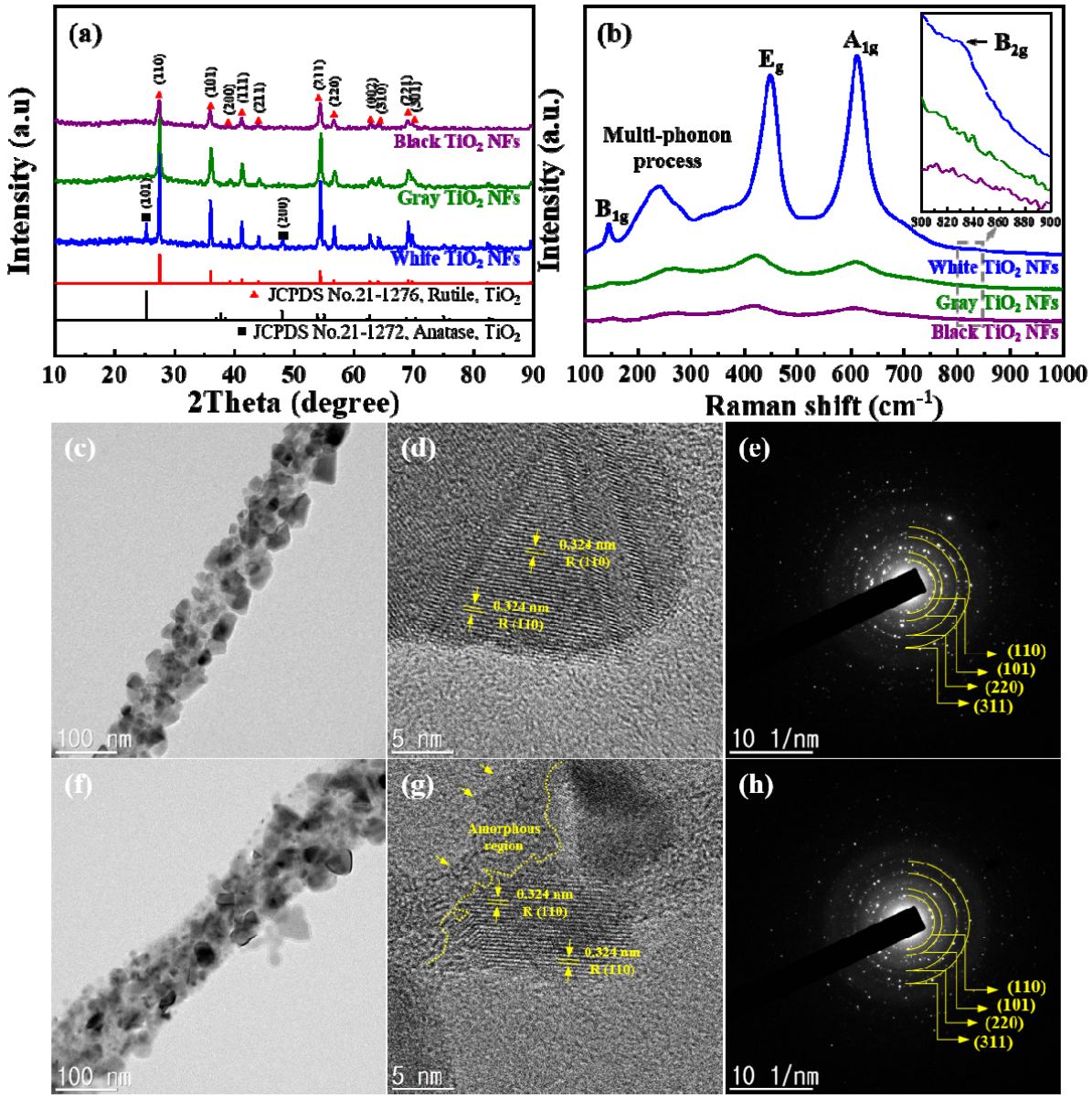

Fig. 3. (a) XRD patterns and (b) Raman spectra of white, gray, and black TiO_2 nanofibers (inset of figure: enlarged Raman spectra). TEM, HR-TEM images and SAEM patterns of (c,d,e) gray and (f,g,h) black TiO_2 nanofibers

The SAED patterns with distinguished rings, presented in Fig. 3(e,h), show that both calcined nanofibers are well-crystallized rutile TiO_2 and have polycrystalline, which is consistent with the above results.

The chemical state of white and black TiO_2 nanofibers was determined by XPS analysis. The high-resolution spectra of Ti 2p state of white TiO_2 nanofibers clearly depict the two peaks centered at 458.8 eV (Ti $2p_{3/2}$) and 464.6 eV (Ti $2p_{1/2}$), which are consistent with the characteristic peaks of Ti^{4+} in the previous literature. On the other hand, in black TiO_2 nanofibers, the chemical shift into lower binding energy and additional peaks centered at 456.8 eV and 462.5 eV are observed, which are ascribed to Ti^{3+} in the lattice. The effect of oxygen vacancies on chemical states is clearly observed in O 1s state (Fig. 4(b)). The O 1s spectrum of black TiO_2 nanofibers clearly shows the shoulder form due to the higher intensity of peak centered at 532.0 eV originating from oxygen vacancies [24-27]. Fig. 4(c) shows the UV-Vis absorption spectra of black and white TiO_2 nanofibers. White TiO_2 exhibits a large absorption at a wavelength shorter than 400 nm, which is attributed to the intrinsic bandgap of anatase TiO_2, but the black TiO_2 distinctly shows an extended absorption range from ultraviolet to near-infrared region. This is consistent with the reported major feature of black TiO_2 by bandgap narrowing attributed to oxygen vacancies [4,10,22,23]. The bandgap of nanofibers was calculated according to the modified Kubelka-Munk function of $(F(R)hv)^{1/2}$ versus the energy of absorbed light and the graphs are plotted in Fig. 4(d,e). The bandgap value for the black TiO_2 is estimated to be 2.67 eV which is smaller than that of white TiO_2 and it is attributed that oxygen vacancies narrow the bandgap of TiO_2 [4,11].

4. Conclusions

In this study, the black TiO_2 nanofibers with an average diameter of 50.3 nm have been successfully synthesized by electrospinning using citric acid and subsequent calcination in the Ar atmosphere. Moreover, it was clearly proved the main characteristics of black TiO_2 such as a disordered surface layer, variation of chemical environment and bandgap narrowing through various analysis tools. Through this study, it was demonstrated a simple route for the synthesis of black TiO_2 nanofibers by the controlled oxidation process using an anoxic atmosphere and antioxidant. It is expected that our present work could provide useful information for future development of synthesizing 1D nanostructured black metal oxides.

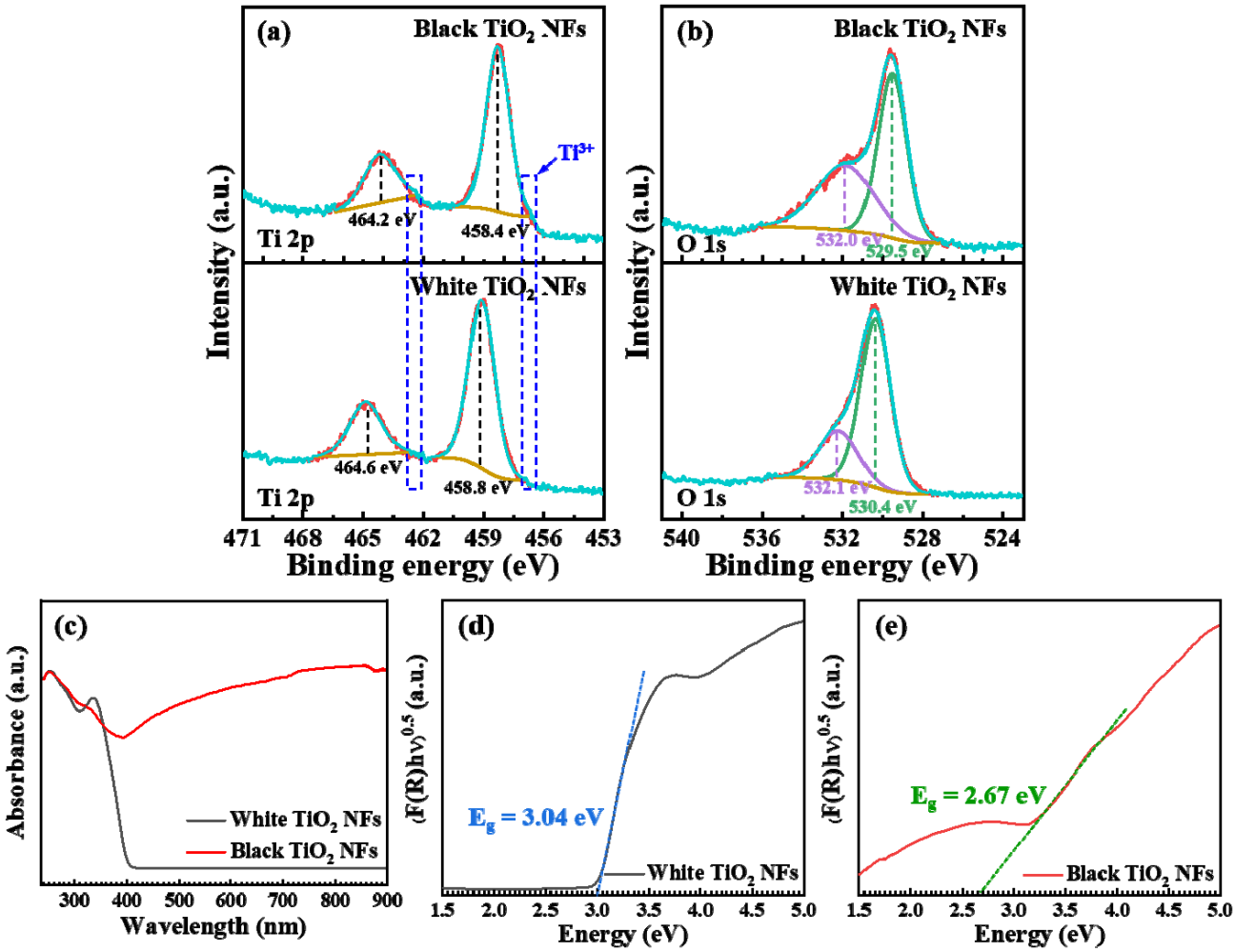

Fig. 4. XPS spectra of white and black TiO_2 nanofibers: (a) Ti 2p (b) O 1s. (c) UV-Vis absorption spectra and (d,e) the Kubelka-Munk plots obtained from UV-Vis diffuse reflectance spectra of white and black TiO_2 nanofibers

Acknowledgments

This study was supported by the Research Program funded by the SeoulTech(Seoul National University of Science and Technology).

REFERENCES

[1] Y. Xia, P. Yang, Y. Sun, Y. Wu, B. Mayers, B. Gates, Y. Yin, F. Kim, H. Yan, Adv. Mater. **15.5**, 353-389 (2003).
[2] G.-D. Lim, J.-H. Yoo, M. Ji, Y.-I. Lee, J. Alloys Compd. **806**, 1060-1067 (2019).
[3] M. Ji, Y.-H. Choa, Y.-I. Lee, Ultrason. Sonochem. **74**, 105557 (2021).
[4] X. Chen, L. Liu, P. Y. Yu, S. S. Mao, Science **331**, 746-750 (2011).
[5] S. Bai, N. Zhang, C. Gao, Y. Xion, Chem. Eng. J. **343**, 708-736 (2018).
[6] I. Zada, W. Zhang, P. Sun, M. Imtiaz, N. Iqbal, U. Ghani, R. Naz, Y. Zhang, Y. Li, J. Gu, Q. Liu, D. Pantelic, B. Jelekovic, D. Zhang, Appl. Mater. Today **20**, 100669 (2020).
[7] S. Kang, T. Im, M. Koh, C. Sunyong, J. CO2 Util. **41**, 101230 (2020).
[8] A. Lepcha, C. Maccato, A. Mettenborger, T. Andreu, L. Mayrhofer, M. Walter, S. Olthof, T.-P. Ruoko, A. Klein, M. Moseler, K. Meerholz, J.R. Morante, D. Barreca, S. Mathur, J. Phys. Chem. C **119**, 18835-18842 (2015).
[9] S. Bai, N. Zhang, C. Gao, Y. Xiong, Nano Energy **53**, 296-336 (2018).
[10] Z. Tian, H. Cui, G. Zhu, W. Zhao, J. Xu, F. Shao, J. He, F. Huang, J. Power sources **325**, 697-705 (2016).
[11] S.G. Ullattil, S.B. Narendranath, S.C. pillai, P. Periyat, Chem. Eng. J. **343**, 708-736 (2018).
[12] S.G. Ullattil, P. Peryat, J. Mater. Chem. A **4**, 5854-5858 (2016).
[13] L.R. Grabstanowicz, S. Gao, T. Li, R.M. Rickard, T. Rajh, D.-J. Liu, T. Xu, Inorg. Chem. **52**, 3884-3890 (2013).
[14] S. Chen, Y. Xiao, Y. Wang, Z. Hu, H. Zhao, W. Xie, Nanomaterials **8**, 245 (2018).
[15] Z. Gu, Z. Cui, Z. Wang, T. Chen, P. Sun, D. Wen, Appl. Surf. Sci. **544**, 148923 (2021).
[16] X. Zhou, E.M. Zolnhofer, N.T. Nguyen, N. Liu, K. Meyer, P. Schmuki, Angew. Chem. **127**, 13583-13587 (2015)
[17] J. Xue, T. Wu, Y. Dai, Y. Xia, Chem. Rev. **119**, 5298-5415 (2019).
[18] Y. Iida, S. Ozaki, J. Am. Ceram. Soc. **44.3**, 120-127 (1961).
[19] H. Albetran, B.H. O'Connor, I.M. Low, Appl. Phys. A **122.4**, 1-9 (2016).
[20] H. Albetran, B.H. O'Connor, I.M. Low, Mater. Des. **92**, 480-485 (2016).
[21] S. Challagulla, K. Tarafder, R. Ganesan, S. Roy, Sci. Rep. **7.1**, 1-11 (2017).
[22] X. Pan, M.-Q. Yang, X. Fu, N. Zhang, Y.-J. Xu, Nanoscale **5**, 3601-3614 (2013).
[23] A. Sinhamahapatra, J.-P. Jeon, J.-S. Yu, Energy Environ. Sci. **8**, 3539-3544 (2015).
[24] L. Han, B. Su, G. Liu, Z. Ma, X. An, Mol. Catal. **456**, 96-101 (2018).
[25] H. Zhang, J. Cai, Y. Wang, M. Wu, M. Meng, Y. Tian, X. Li, J. Zhang, L. Zheng, Z. Jiang, J. Gong, Appl. Catal. B **220**, 126-136 (2018).
[26] Y. Xu, H. Li, B. Sun, P. Qiao, L. Ren, G. Tian, B. Jiang, K. Pan, W. Zhou, Chem. Eng. J. **379**, 122295 (2020).
[27] A. Sarkar, G.G. Khan, Nanoscale **11**, 3414-3444 (2019).